Title	Modelling the degradation and elastic properties of poly(lactic-co-glycolic acid) films and regular open -cell tissue engineering scaffolds
Author(s)	Shirazi, Reyhaneh Neghabat; Ronan, William; Rochev, Yury; McHugh, Peter
Publication Date	2015-09-02
Publication Information	Shirazi, RN,Ronan, W,Rochev, Y,McHugh, P (2016) 'Modelling the degradation and elastic properties of poly(lactic-co-glycolic acid) films and regular open -cell tissue engineering scaffolds'. Journal Of The Mechanical Behavior Of Biomedical Materials, 54 :48-59.
Publisher	Elsevier
Link to publisher's version	http:/dx.doi.org/doi:10.1016/j.jmbbm.2015.08.030
Item record	http://hdl.handle.net/10379/5933
DOI	http://dx.doi.org/10.1016/j.jmbbm.2015.08.030

Modelling the degradation and elastic properties of poly(lactic-co-glycolic acid) films and regular open-cell tissue engineering scaffolds

Reyhaneh Neghabat Shirazi[1,#], William Ronan[1], Yury Rochev[2,3,*], Peter McHugh[1,*]

[1]Biomechanics Research Centre (BMEC), Biomedical Engineering, College of Engineering and Informatics, National University of Ireland Galway, Ireland

[2]School of Chemistry, National University of Ireland Galway, Ireland

[3]National Centre for Biomedical Engineering Science (NCBES), National University of Ireland Galway, Ireland

[*]Joint senior author

[#]Corresponding author

Email: r.neghabatshirazi1@nuigalway.ie

Tel: +353 (0)91 492723

Fax: +353 (0)91 563991

Nomenclature

C_e	mole concentration of ester bonds of polymer chains	N_0	initial number of polymer chains
C_{e0}	initial mole concentration of ester bonds of polymer chains	N_{total}	sum of polymer units in a group of chains
C_m	mole concentration of monomers	n	total number of chains in a group of chains
k_1	non-catalytic reaction rate constant	N_{chains}	total number of polymer chains
k_2	autocatalytic reaction rate constant	$R_{scissions}$	ratio of random scissions to end scissions
k	Boltzmann's constant	T	absolute temperature
D	effective diffusion coefficient	A_0	initial total cross sectional area
D_0	intrinsic diffusion coefficient	A_{free}	free surface
$\overline{D}$	dimensionless diffusion coefficient	σ_0	nominal stress
β	dissociation power of the acid end group	ε_A	nominal strain
α	diffusion porosity constant	F_R	reaction force
M_n	number average molecular weight of polymer	E	Young's modulus
M_{n0}	initial number average molecular weight of polymer	E_0	initial Young's modulus
$\overline{M}_n$	averaged-volume of number average molecular weight of polymer	$E_{effective}$	effective modulus
M_n^{crit}	critical number average molecular weight of polymer	E^*	normalised effective modulus
M_0	molar mass	l_{char}	characteristic diffusion length
N	number of polymer chains	l_{diff}	diffusion length

Abstract

Scaffolding plays a critical rule in tissue engineering and an appropriate degradation rate and sufficient mechanical integrity are required during degradation and healing of tissue. This paper presents a computational investigation of the molecular weight degradation and the mechanical performance of poly(lactic-co-glycolic acid) (PLGA) films and tissue engineering scaffolds. A reaction-diffusion model which predicts the degradation behaviour is coupled with an entropy-based mechanical model which relates the Young's modulus and the molecular weight. The model parameters are determined based on experimental data for in-vitro degradation of a PLGA film. Microstructural models of three different scaffold architectures are used to investigate the degradation and mechanical behaviour of each scaffold. Although the architecture of the scaffold does not have a significant influence on the degradation rate, it determines the initial stiffness of the scaffold. It is revealed that the size of the scaffold strut controls the degradation rate and the mechanical collapse. A critical length scale due to competition between diffusion of degradation products and autocatalytic degradation is determined to be in the range 2-100 µm. Below this range, slower homogenous degradation occurs; however, for larger samples monomers are trapped inside the sample and faster autocatalytic degradation occurs.

Keywords: PLGA; Degradation; Finite element modelling; Tissue engineering scaffold; Mechanical properties; Size effect

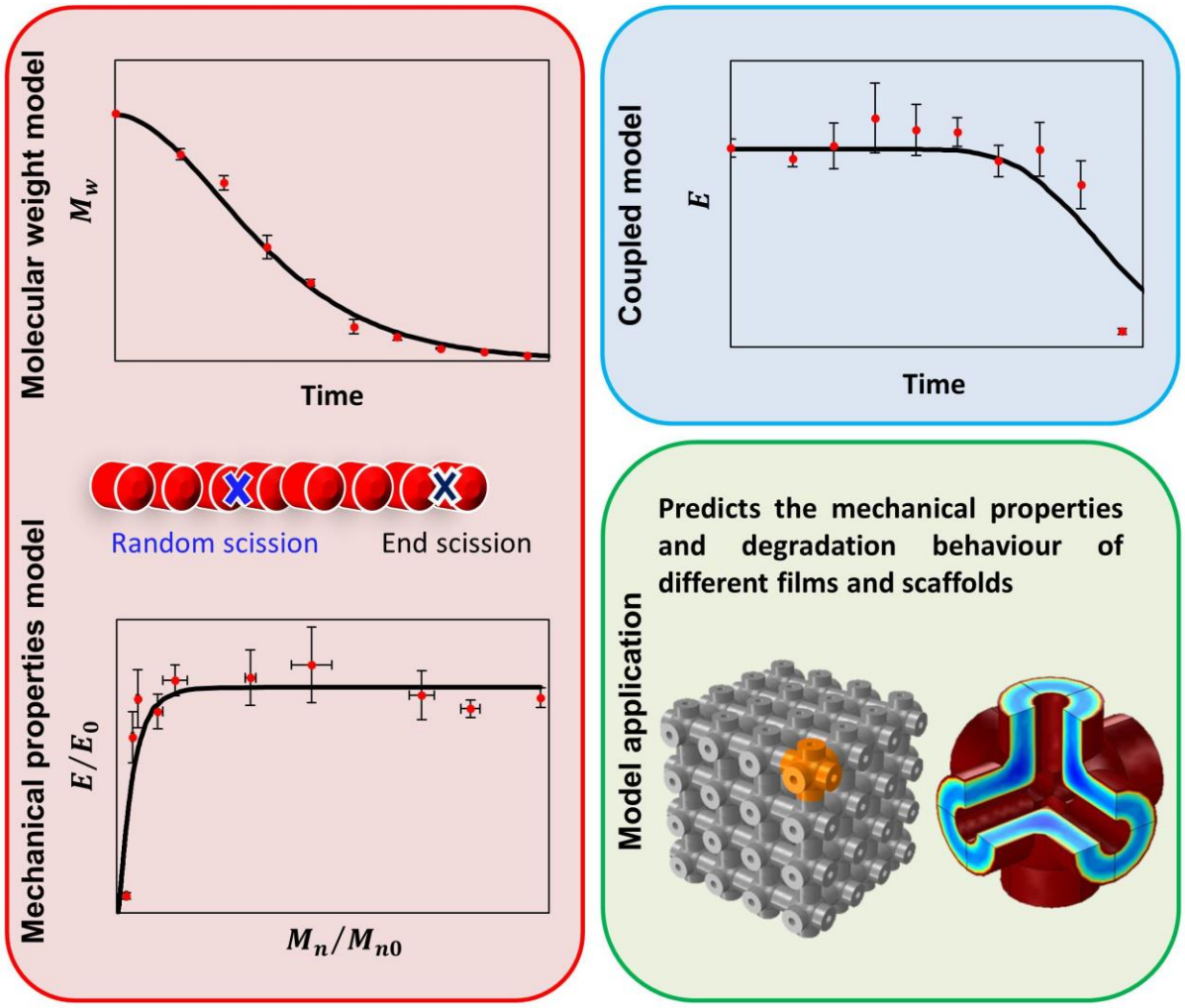

1 Introduction

It is well known that scaffolding plays a critical role in tissue engineering. Biodegradable polymers have been used widely to provide a three-dimensional structure that facilitates tissue regeneration and wound healing (Cheng et al., 2013; Harada et al., 2014; Ren et al., 2005; Uematsu et al., 2005). The degradation process of biodegradable polyesters such as poly(lactic-co-glycolic acid) (PLGA) is based on a hydrolytic reaction. Diffusion of water causes hydrolysis of the ester bonds in the polymer chains, leading to the generation of water soluble oligomers. Consequently, the molecular weight of the polymer decreases. The degradation products diffuse into the surrounding medium, which results in a mass loss for the polymer (Pamula and Menaszek, 2008; Shirazi et al., 2014; Vey et al., 2012).

Diffusion of the degradation products may occur more slowly in a large-sized sample due to the greater diffusion length (Dunne et al., 2000; Grayson et al., 2005; Grizzi et al., 1995; Lu et al., 1999; Witt and Kissel, 2001). This leads to accumulation of degradation products inside the polymer matrix, which are able to catalyse hydrolysis of the other ester bonds and consequently accelerates the degradation process. This phenomenon is called autocatalysis. Therefore, due to the autocatalytic effect the large PLGA samples undergo a heterogeneous degradation with a degradation rate which is greater at the centre than at the surface.

In order to support tissue formation, the scaffold should retain sufficient stability during degradation. A clear understanding of the evolution of the mechanical properties of PLGA scaffolds during degradation is required. Towards this, computational modelling offers an efficient framework to understand the behaviour of biodegradable implants. Many models have been proposed to describe the degradation of biodegradable polymers (Sackett and Narasimhan, 2011) including PLGA (Ford Versypt et al., 2013). Reaction-diffusion models have been applied to a range of aliphatic polyesters. Among these models, the ones which account for the autocatalytic effect are the most comprehensive, as autocatalysis plays a strong role in the degradation mechanism (Chen et al., 2011; Ford Versypt et al., 2013; Wang et al., 2008).

A number of models have been presented to predict the mechanical properties of degradable polymers (Hayman et al., 2014; Soares et al., 2010; Vieira et al., 2014; Vieira et al., 2011; Wang et al., 2010). A model was developed by Vieira *et al.* (2014) based on the relationship between fracture strength and molecular weight for thermoplastic polymers to predict the mechanical properties of PLA-PCL fibers during degradation. Since this model is based on an empirical equation, the model parameters must be determined experimentally for each material and during degradation. Also, in this model, the hydrolytic degradation rate is assumed constant, which is a significant simplification for highly heterogeneous degradation as autocatalysis has a significant effect on degradation.

The model of Soares *et al.* (2010) relates the degradation rate to the mechanical deformation in order to determine the mechanical properties of poly(L-lactide) (PLLA) fibres loaded under uniaxial extension. The degradation behaviour is determined from a thermodynamic analysis of the degradation process and as degradation proceeds the material loses its ability to store energy.

Despite the fact that the degradation of PLGA polymers results in a quick decrease in the polymer molecular weight, the Young's modulus does not decrease until the number of polymer chains reaches a critical molecular weight (Shirazi et al., 2014). Wang *et al.* (2010) proposed a model for amorphous biodegradable polymers, based on the relationship between the Young's modulus and the number of polymer chains. This model is physically motivated by the hydrolytic random scission of the polymer chains. The model assumes that the number of polymer chains above a critical molecular weight determines the Young's modulus as chain scissions occur. This model successfully predicted the experimental observed degradation of PLLA films.

Motivated by recent developments, an integrated modelling framework based on the work of Wang *et al.* (2010; 2008) was developed in the current study to predict the degradation of biodegradable

polymers and, in particular, PLGA. The first objective of this study was to develop a computational framework that links both of the key physical processes: the reduction in molecular weight over time during degradation; and the relationship between Young's modulus and molecular weight (and polymer chain length). The second objective was to calibrate the models based on the experimental data for in-vitro degradation of a PLGA film. The third objective was to predict the molecular weight and the reduction in Young's modulus for PLGA films of different thicknesses and also for a range of PLGA scaffolds. The effect of strut size and architecture of the scaffold on the degradation rate and the mechanical performance were investigated.

2 Methods

This section is organised as follows: an overview of the phenomenological degradation model of Wang *et al*. (2010), which predicts the changes in the molecular weight distribution during degradation, is presented (hereafter referred to as the molecular weight model); the entropy spring model which relates Young's modulus to the molecular weight distribution is described (hereafter referred to as the mechanical properties model); the coupling of these two models is then described; and finally we outline the simulations performed in the current study. An overview of each model and the coupling scheme is shown in Figure 1.

2.1 Molecular weight model

In the current study, a phenomenological model developed by Wang *et al.* (2008) was used to predict the reduction in molecular weight of PLGA polymers. In this model, the molecular weight distribution of the polymer is described by the mole concentration of polymer ester bonds, C_e, which remain inside the polymer matrix, and the mole concentration of monomers, C_m. Monomers are produced during the hydrolytic reaction and they can diffuse throughout the polymer and also into the surrounding aqueous medium. The rate of change of C_e is determined by the hydrolytic reactions (including non-catalytic and autocatalytic reactions) of the polymer chains.

The degradation behaviour of biodegradable polymers is captured by the following reaction-diffusion equations (Wang et al., 2008):

$$\frac{dC_m}{dt} = k_1 C_e + k_2 C_e C_m^{\beta} + \nabla \cdot (D \nabla C_m) \tag{1}$$

$$\frac{dC_e}{dt} = -\left(k_1 C_e + k_2 C_e C_m^{\beta}\right) \tag{2}$$

where k_1 and k_2 are the reaction rate constants for the non-catalytic and autocatalytic reactions, respectively, and the final term in Eq. (1) is the divergence of the gradient of C_m accounts for the diffusion of monomers. The exponent β captures the non-linearity of the autocatalytic reaction, and accounts for dissociation of the acid end group. The effective diffusion coefficient D is:

$$D = D_0 \left[1 + \alpha \left(1 - \frac{C_m + C_e}{C_{e0}}\right)\right] \tag{3}$$

where D_0 is an intrinsic diffusion coefficient, C_{e0} is the initial value of C_e, and α is a constant equal to 4.5 (Wang et al., 2008).

The average molecular weight of the polymer is calculated based on concentration of ester bonds. It is assumed that the monomers are too small to detect. Therefore, the number average molecular weight, M_n, can be related to C_e as follows:

$$\frac{M_n}{M_{n0}} = \frac{C_e}{C_{e0}} \quad (4)$$

where M_{n0} is the initial number average molecular weight.

The numerical solution of Eqs. (1) to (3) was obtained by implementation in a finite element formulation using Comsol Multiphysics v4.3b. These equations were solved at each time step in each element resulting in the concentration of ester bonds of the polymer with time. The degradation of the polymer was then determined by the number average molecular weight of the polymer according to Eq. (4).

2.2 Mechanical properties model

The Young's modulus (E) of a polymer network can be related to the number of polymer chains per unit volume, N, (Ward and Sweeney, 2012):

$$E = 3NkT \quad (5)$$

where k is the Boltzmann's constant and T is the absolute temperature. This theory was modified by Wang *et al.* (2010) by assuming that scissions of very long chains (which are constrained by surrounding chains) do not significantly affect the entropy change and, hence, N. Also, it was assumed that a chain with molecular weight smaller than a critical molecular weight is not included in counting the number of chains and consequently does not contribute to the polymer stiffness. Thus, N only decreases from its initial value; the Young's modulus does not increase during degradation.

Polymer chains are affected by two degradation processes, similar to those described in Eqs. (1) and (2): polymer chain end scission (where scission occurs at the final bond at chain ends resulting in the production of a monomer) and random chain scission (where scission occurs randomly at any bond in a chain resulting in production of two chains with random lengths). An initial distribution of chains is assumed and, after each scission, the lengths of each newly produced chain are stored. The ratio of random scissions to end scissions ($R_{scissions}$) determines how often each type of scission occurs.

Each original chain and the resulting shorter chains are counted as one chain (with respect to Eq. (5)). Once the number average molecular weight (M_n) falls below a critical molecular weight, M_n^{crit}, the group of chains does not contribute to the stiffness and is no longer counted. For each group of chains, M_n is calculated as the total weight of all chains divided by the number of chains:

$$M_n = \frac{N_{total} M_0}{n} \quad (6)$$

where N_{total} is the sum of polymer units in a group, M_0 is the average molar mass of poly(lactide) and poly(glycolide) (65 g mol^{-1}), and n is the total number of chains in the group.

The random occurrence of the scissions and the subsequent evolution of the molecular weight distribution, i.e. the lengths of the chains, were predicted using Matlab (R2014a, Mathworks, MA, U.S.A.). The mechanical properties model thus predicts a non-linear decrease in Young's modulus as M_n decreases.

An initial distribution of the polymer molecular weight was obtained from the experimental gel permeation chromatography (GPC) curve for a PLGA film (Shirazi et al., 2014). The total number of polymer chains (N_{chains}) was chosen and then the lengths of these chains were determined such that the molecular weight of the chains in the simulation matched the experimental GPC data. The sensitivity of the model to the initial conditions (N_{chains}, $R_{scissions}$, and M_n^{crit}) was assessed and is described in Section 3.1.

2.3 Simulation procedure

2.3.1 Coupling molecular weight and mechanical properties models

The molecular weight model (described in section 2.1) and the mechanical properties model (defined in section 2.2) were coupled in order to simulate the mechanical behaviour of PLGA during degradation. The change in the molecular weight distribution as polymer chains undergo scissions was captured in Comsol for the various films and scaffolds defined later. As the degradation proceeded, the molecular weight distribution at each solution point was updated. This distribution was represented in Comsol via the variables C_e and C_m, i.e. the concentrations of esters bonds and monomers.

At each time step, the mechanical properties model was then used to calculate the current modulus at each integration point. As described in Eq. (4), changes in C_e are assumed to capture changes in M_n. Thus, changes in C_e (as predicted by the molecular weight model) were related (via the mechanical properties model) to changes in the Young's modulus. Finally, the distribution of E was used as the input to further finite element simulations of PLGA scaffolds under mechanical loading.

2.3.2 Model applications

The coupling framework described above was used in a one-dimensional model for PLGA films and in a three-dimensional model for PLGA scaffolds. The degradation of PLGA films was represented with a one-dimensional model as the diffusion of degradation products occurs only in the direction normal to the free surface.

Contact on the outside of the film with the aqueous medium was represented by assuming the concentration of monomers at the boundary of the film is zero (C_m=0), which means that all the monomers which reached the surface are immediately convected away from the surface by the environmental flow. The flux of monomers at all other boundaries, including the interface between the film and the substrate, was set to zero.

In the second part of the study, microstructural models of three different scaffold architectures were used, based on those used in the literature (Bucklen et al., 2008; Luxner et al., 2005; Wettergreen et al., 2005). Unit cells for different architectures were generated for each scaffold, as shown in Figure 2. The porosity of each scaffold was kept at 63.5% by keeping the ratio of strut dimensions to unit cell size constant as the strut size was varied. Due to the symmetry of the scaffold geometry, only one-eighth of the unit cell was needed to generate the representative volume element (RVE) in each case, as shown in green in Figure 2. Table 1 shows the dimensions for the three scaffolds with the same strut thickness. Similar to the film simulations, C_m was set to zero on the free surface in contact with the aqueous medium (which are highlighted in red in Figure 2). The interior of the scaffolds were meshed with tetrahedral elements and thinner boundary layer elements were used at the surfaces where higher gradients in the solution variables occur.

In order to estimate the effective modulus of the degraded scaffold, uniaxial compression of the RVE was simulated. Periodic and symmetry boundary conditions were applied such that the faces on the boundaries of the RVE remained planar and parallel. A uniaxial compressive strain was applied in the Z direction and the RVE was free to expand or contract in the X and Y directions. As the applied strain was small (< 1%), buckling of the structure was not considered and geometric nonlinearities from large displacement were neglected. The material was assumed to be isotropic with a Poisson's ratio of 0.3. The effective modulus ($E_{effective}$) was then calculated:

$$E_{effective} = \frac{\sigma_0}{\varepsilon_A}; \quad \sigma_0 = \frac{F_R}{A_0} \tag{7}$$

where σ_0 is the nominal stress on the loaded face of the RVE, ε_A is the applied nominal strain, A_0 is the initial total cross sectional area of the loaded face, and F_R is the resultant reaction force on the

loaded face. In order to compare the degradation in stiffness of different scaffolds, the results were normalised by the initial Young's modulus of the solid cube (E_0):

$$E^* = \frac{E_{effective}}{E_0} \quad (8)$$

Finally, in order to compare the predictions of the molecular weight model for different scaffold geometries and films, a volume-averaged molecular weight is defined as:

$$\bar{M}_n = \frac{1}{V}\int_V M_n dV \quad (9)$$

3 Results

3.1 Model calibration

The parameters of the molecular weight model (k_1, k_2, and D_0) and the mechanical properties model (N_{chains}, $R_{scissions}$, and M_n^{crit}) were calibrated to fit the experimental data obtained by Shirazi *et al.* (2014) which described the reduction in the molecular weight and the Young's modulus for a PLGA (50:50) film (with a thickness of 250 µm) degraded in a phosphate buffer solution, pH 7.4 at 37°C.

Figure 3 (A, B, C) compares the $\bar{M}_n$ experimental data with different combinations of parameters for the molecular weight model. The ratio of k_1 to k_2 was set at 1, 5, and 50. An initial number average molecular weight (M_{n0}) of 82000 g mol^{-1} was assumed and the initial concentration of ester bonds (C_{e0}) was set at 17300 mol m^{-3} (Wang et al., 2008).

The next step of the calibration is to determine the correct value of M_n^{crit} so that the mechanical properties model correctly predicts the experimentally observed relationship between normalised E and M_n, as shown in Figure 4. The best model fitting to the experimental data was achieved using N_{chains}=3000 polymer chains and M_n^{crit}=1500 g mol^{-1}. For less than 3000 polymer chains (300, 500, or 1000), the molecular weight of the chains in the simulation was not matched the experimental GPC data. For more than 3000 polymer chains (10,000 or 20,000), similar results were achieved (data not shown). Different values of random to end scission ratios (3:1, 1:1, 1:12 or 1:50) did not show any significant effect on the results (data not shown).

Finally, Figure 3 (D, E, F) shows the prediction for E as a function of time using the coupled molecular weight and mechanical properties model. Comparing the curves for $\bar{M}_n$ versus time and the curves for E versus time (Figure 3), the best fitting was achieved by β=0.5, k_1=0.002 day^{-1}, k_2=0.002 (m^3 mol^{-1})$^{0.5}$ day^{-1}, and D_0=10^{-12} m^2 day^{-1}. The computational model correctly predicted the experimentally observed decrease in $\bar{M}_n$ and E.

3.2 Effect of thickness on the Young's modulus of PLGA films

The coupled model was used to investigate the effect of film thickness on degradation behaviour. Figure 5A shows the predicted changes in $\bar{M}_n$ with time for PLGA films with thickness ranging from 0.25 to 2500 µm over 40 days, as predicted by the molecular weight model. $\bar{M}_n$ for films thicker than 2.5 um was predicted to decrease rapidly over the first 10 days, after which the rate of degradation slowed significantly. After 20 days, the thicker films had almost completely degraded. In contrast, the 2.5 µm film has only degraded by 50% and the 0.25 µm film was still 95% of the initial value. The rate of change of $\bar{M}_n$ for the thinnest film is consistent with purely homogenous degradation (i.e. $d\bar{M}_n/dt = -k_1\bar{M}_n(t=0)$).

The combined model was then used to predict the changes in E of the film as a function of time, as shown in Figure 5B. The Young's modulus is predicted to remain at the initial value until day 13, after

which the thicker films underwent a rapid decrease in stiffness. For films larger than 2.5 μm, a significant reduction in Young's modulus did not begin until after ~13 days; however, for films smaller than 2.5 μm the Young's modulus did not reduce even after 40 days. For films thicker than 50 μm, the stiffness after 25 days was less than 10% of the initial value and the fastest decrease was predicted for the thickest 2500 μm film, which had lost all structural stiffness after 25 days.

As shown above in Figure 4, there is a highly non-linear relationship between modulus and molecular weight. Therefore it is possible to have a significant decrease in $\bar{M}_n$, e.g by 50% for the 2.5 μm film, without a significant decrease in E. Once the molecular weight drops below the critical level shown in Figure 4 (M_n/M_{n0} < 0.2), the polymer chains have undergone a significant amount of scissions such that the decrease in polymer chain entanglement causes a drop in stiffness, as shown in Eq. (5) and discussed above in section 2.2. Thus the 2.5 μm film has sufficiently long chains to retain close to its initial stiffness, while the larger films have a lower molecular weight and the shorter chains give the polymer a lower stiffness.

3.3 Degradation behaviour and effective elastic modulus for PLGA scaffolds

Next, degradation of PLGA scaffolds was predicted using the same model parameters as calibrated above for films. The predicted distribution of M_n for the scaffolds with 0.05 mm thick struts after 25 days of degradation is shown in Figure 6. The contour plots show that the molecular weight degradation was faster in the centre of the scaffold unit cells, as these are the areas in the scaffold that are furthest from a free surface. This demonstrated the heterogeneous bulk degradation of the scaffolds with 0.05 mm struts.

Figure 7A shows that the volume averaged molecular weight $\bar{M}_n$ was the same for the three different scaffold geometries with strut size of 0.05 mm. The decrease in $\bar{M}_n$ began immediately at day 0 and continued approximately linearly until day 10, when the rate of degradation slowed significantly. $\bar{M}_n$ was approximately zero after 30 days. The decrease in $\bar{M}_n$ was not affected by the scaffold architecture; however these scaffolds had a strut thickness of 0.05mm (the effect of strut thickness is discussed below). In contrast to the decrease in molecular weight, which began at day 0, the effective modulus of each of the scaffolds did not decrease until ~13 days, as shown in Figure 7B. Although the initial stiffness of each scaffold was strongly affected by the architecture; scaffold A was initially twice as stiff as the other two scaffolds.

Finally, the effect of strut thickness was investigated for each PLGA scaffold. Figure 8 shows $\bar{M}_n$ and E^* for each scaffold with strut sizes ranging from 0.002 to 1 mm (note that the porosity of all scaffolds was kept fixed at 63.5% by varying the size of the unit cell). For each scaffold geometry, increasing the thickness from the 0.05 mm scaffolds shown in Figures 6 and 7 did not alter either the volume averaged molecular weight (Figure 8 (A, B, C)), or the effective modulus (Figure 8 (D, E, F)). In contrast, decreasing the thickness significantly changed the behaviour. For the thinnest strut size, the degradation was slowed such that there was no change in E^* after 40 days. For intermediate strut thickness, the rate of decrease in $\bar{M}_n$ and E^* was slower than for the thick 0.05 mm struts.

In order to illustrate how the degradation mechanism is affected by the strut thickness, the variation of M_n through the thickness of a strut for scaffold B is shown in Figure 9. The data is shown as a function of the dimensionless coordinate R/R_0 (where R_0 is the radius of the strut; R/R_0 is 0 at the centre of the strut and 1 at the free surface). For the scaffolds with thick struts (> 0.05 mm), is significantly lower in interior of the strut and there is a very steep gradient in M_n near the surface, clearly showing the heterogeneous nature of the degradation. In contrast, for the thinnest strut, M_n only varies by ~15% between the surface and the interior of the scaffold, showing that the degradation is homogenous.

4 Discussion

The current study presents a computational investigation of the molecular weight degradation and the mechanical performance of PLGA films and tissue engineering scaffolds. We developed a computational framework to couple a reaction-diffusion model that captures changes in molecular weight distribution during degradation to a polymer chain model that captures the relationship between the molecular weight distribution and the mechanical properties. The model framework was calibrated based on experimental data for the in-vitro degradation of a PLGA film. The calibrated model was then used to predict the molecular weight and the reduction in Young's modulus for PLGA films of different thicknesses and also for a range of PLGA scaffolds.

This study demonstrates the importance of the autocatalytic hydrolysis on the degradation rate of PLGA films. The results calibration results have shown that the autocatalytic reaction constant (k_2) has a significant effect on M_n and the degradation rate is much faster for the higher values of k_2; in contrast, the effect of the non-catalytic reaction constant (k_1) is small. This suggests that, in our case, the autocatalytic hydrolysis is the dominant degradation mechanism in PLGA.

As the modulus is non-linearly dependent on the molecular weight, the degradation rate thus has a non-linear effect on the stiffness. The length of the polymer chains decreases as the PLGA degrades via end scissions and random scissions. Following from Eq. (5), once the polymer chains are shortened sufficiently during degradation, there is a sudden change in Young's modulus. This causes the collapse in stiffness seen for the film and scaffold compression.

In the present study, the Young's modulus was predicted to decrease faster for thicker PLGA films. Computed predictions correlate strongly with published experimentally observed trends of degradation for the PLGA devices with different sizes. Some authors have studied the degradation rates for PLGA devices 200 µm to as small as 0.53 µm in size (Dunne et al., 2000; Grayson et al., 2005; Grizzi et al., 1995; Lu et al., 1999; Witt and Kissel, 2001). In these studies, it has been observed frequently that the degradation time is significantly shorter in the thicker samples due to the autocatalytic effect of the degradation products. In the latter part of the current study, the combined model is used to investigate the degradation of different scaffold geometries. For larger strut sizes, autocatalytic heterogeneous degradation occurs and the scaffolds are shown to mechanically collapse after 13 days. In contrast, simulations predict that the degradation rate of the scaffold is much slower when the strut size of the scaffold is smaller than 0.05 mm.

These results are consistent with the experimental results obtained by Wu *et al.* (2005) for in-vitro degradation of PLGA porous scaffolds. Saito *et al.* (2013; 2012) has studied the effect of the strut size on in-vivo degradation of poly(L-lactic acid) and PLGA three-dimensional porous scaffolds and demonstrated that scaffolds with larger struts (~0.9 mm) degrade more rapidly than scaffolds with smaller struts (~0.4 mm). The present study elucidates the relationship between the strut size, scaffold architecture, and the stiffness of the scaffold during degradation. This study highlights that the architecture of the scaffold does not have a significant influence on the degradation rate; however, the initial stiffness of the scaffold is strongly influenced by the architecture. It is demonstrated that the effective modulus of the scaffold is substantially dependent on the volume fraction. The simulations predict that different scaffold architectures with the same strut size collapse at approximately the same time.

In the very small scaffolds and films simulated in the current study, the degradation is shown to be homogenous with little variation in M_n through the thickness of the strut. In the smaller samples, the oligomers, which are created as degradation products, can quickly escape from the surface into the aqueous medium. Consequently, the possibility of autocatalysis is very limited for thinner samples and therefore the Young's modulus for thinner samples decreases slower. In contrast, for larger struts and films, the degradation is shown to be autocatalytic with a steep gradient in M_n between the core and the surface of the sample

In order to compare the different scaffold geometries and films, we can consider a characteristic diffusion length given by the volume divided by the free surface area (i.e. the surface in contact with the aqueous medium):

$$l_{char} = \frac{V}{A_{free}} \tag{10}$$

Figure 10A shows the relative change in effective modulus after 25 days for different sizes of each scaffold, where the size of the scaffold is represented by l_{char} (instead of strut thickness). By using this diffusion length scale to describe the size of each scaffold and film, a single trend is elucidated which does not depend on sample shape. For l_{char} < 2 μm, the degradation is homogenous and there is no change in the Young's modulus. For l_{char} > 100 μm, the scaffold has completely degraded and the behaviour is similar for larger samples. Recall that in Figure 8 there is no change in the degradation behaviour for the larger scaffolds and also that Figure 9 shows the degradation of large scaffolds is heterogeneous with a steep gradient in M_n. For intermediate values of l_{char}, there is a smooth transition between these two plateaus.

The sample size at which this transition between homogenous and heterogeneous behaviour occurs is related to the competition between diffusion of monomers and autocatalysis due to high concentrations of monomers in the interior of the sample. The length scale l_{diff} associated with this competition is determined from the material parameters (from the latter part of Eq. (2)):

$$l_{diff} = \sqrt{\frac{D_0}{k_2\sqrt{C_{e0}}}} \tag{11}$$

The calibration in the current study suggests that, l_{diff} ≈ 2 μm. Therefore, when $l_{char} < l_{diff}$, the concentration of monomers remains low due to rapid diffusion, and thus the degradation is homogenous, i.e. the term associated with k_1 dominates Eq. (2). For larger scaffolds, the critical diffusion length l_{diff} is much smaller than the characteristic length; thus the monomers remain trapped in the scaffold and autocatalysis (i.e. the part of Eq. (2) associated with k_2) is the dominant mechanism. Furthermore, the competition between diffusion and autocatalysis can be summarised using the following dimensionless group:

$$\overline{D} = \frac{D_0}{k_2 l_{diff}^2\sqrt{C_{e0}}} \tag{12}$$

As shown superimposed on Figure 10A, when $\overline{D}$ > 1 the degradation is homogenous and when $\overline{D}$ << 1, the degradation is heterogeneous. In the case of the homogenous degradation, it should also be noted that the time constant associated with the non-catalytic degradation is on the order of 500 days.

In Figure 10B, the homogenous, heterogeneous, and transition regimes predicted in the current study are compared to experimental observations of homogenous and heterogeneous diffusion in different sized samples (Chen et al., 1997; Grizzi et al., 1995; Lu et al., 1999; Park, 1995; Shirazi et al., 2014; Spenlehauer et al., 1989; Vey et al., 2008). Grizzi *et al*. (1995) has proposed a range of 200-300 μm as a critical thickness above which the poly(D,L-lactic acid) polymers (plate, film, microsphere)(which have a similar chemical structure and degradation behaviour to PLGA) undergo heterogeneous degradation. The heterogeneous degradation of PLGA films with thicknesses of 300 μm, 250 μm, and 5-100 μm has been shown by Vey *et al.* (2008), Shirazi *et al.* (2014), and Lu *et al.* (1999), respectively. Spenlehauer *et al.* (1989) has showed that PLGA microspheres less than 200 μm in diameter undergo a homogeneous degradation. However, Park *et al.* (1995) has shown the heterogeneous degradation of PLGA microspheres with diameters less than 10 μm. The heterogeneous degradation of PLGA microspheres has been also demonstrated in a study by Chen *et al.* (1997) for PLGA microspheres with diameters of 50-70 μm. While the predictions in the current study are in broad agreement with observations, the disparities in experimentally observed critical

length for transition between heterogeneous and homogenous degradation highlight the need for further experimental investigation of both the mechanical and molecular behaviour of PLGA during degradation.

The PLGA scaffolds in the current study are shown to have a rapid change in stiffness. While it is not clear what the optimal rate of mechanical degradation should be, Heljak *et al.* (2012) explore the performance of multiple material scaffolds to provide a tuneable degradation response. Fast degradation may affect negatively on cell viability and cell migration into the scaffold due to the acidic degradation products as a result of autocatalysis (Sung et al., 2004). Scaffold manufacturing methods have also been shown to have an effect on degradation; a poly(D,L-lactide) (PDLLA) electrospun fibrous mat degrades slower than the PDLLA film prepared by solvent casting and the electrospun mat shows a surface erosion pattern rather than a typical bulk degradation (Cui et al., 2008). As the current study has shown the importance of the free surface area, the slower degradation of the electrospun mat may be due to faster diffusion of the autocatalytic degradation products.

Conclusion

This study used a numerical model that couples changes in molecular weight caused by degradation to the mechanical properties of PLGA. The predictions presented here show that heterogeneous degradation occurs in PLGA when the length scale of the PLGA sample results in a diffusion limited regime where autocatalysis is the dominant degradation mechanism. Consequently, scaffolds with thicker struts demonstrate a higher degradation rate due to stronger autocatalysis and they collapse more rapidly. The presented results show that the architecture of the scaffold does not strongly influence the degradation rate but that it determines the initial stiffness of the scaffold. The computational framework and the insight provided in the current study will be useful in improving the design of biomedical scaffolds.

Acknowledgments

Funding support was provided by the Structured PhD Programme in Biomedical Engineering and Regenerative Medicine (BMERM). Funded under the Programme for Research in Third-Level Institutions (PRTLI) Cycle 5 Strand 2 BMERM and co-funded under the European Regional Development Fund (ERDF).

Table 1: Dimensions for the three scaffolds with the strut thickness of 0.02 mm

Scaffold	Thickness (mm)	$\boldsymbol{L}$ (μm)	$\boldsymbol{R_o}$(μm)	$\boldsymbol{R_i}$(μm)	$\boldsymbol{R_{cyl}}$(μm)	$\boldsymbol{R_{sphere}}$(μm)
A	0.02	60	15	5	n/a	22.72
B	0.02	60	10	n/a	n/a	25.38
C	0.02	60	10	n/a	6.38	n/a

Figure captions

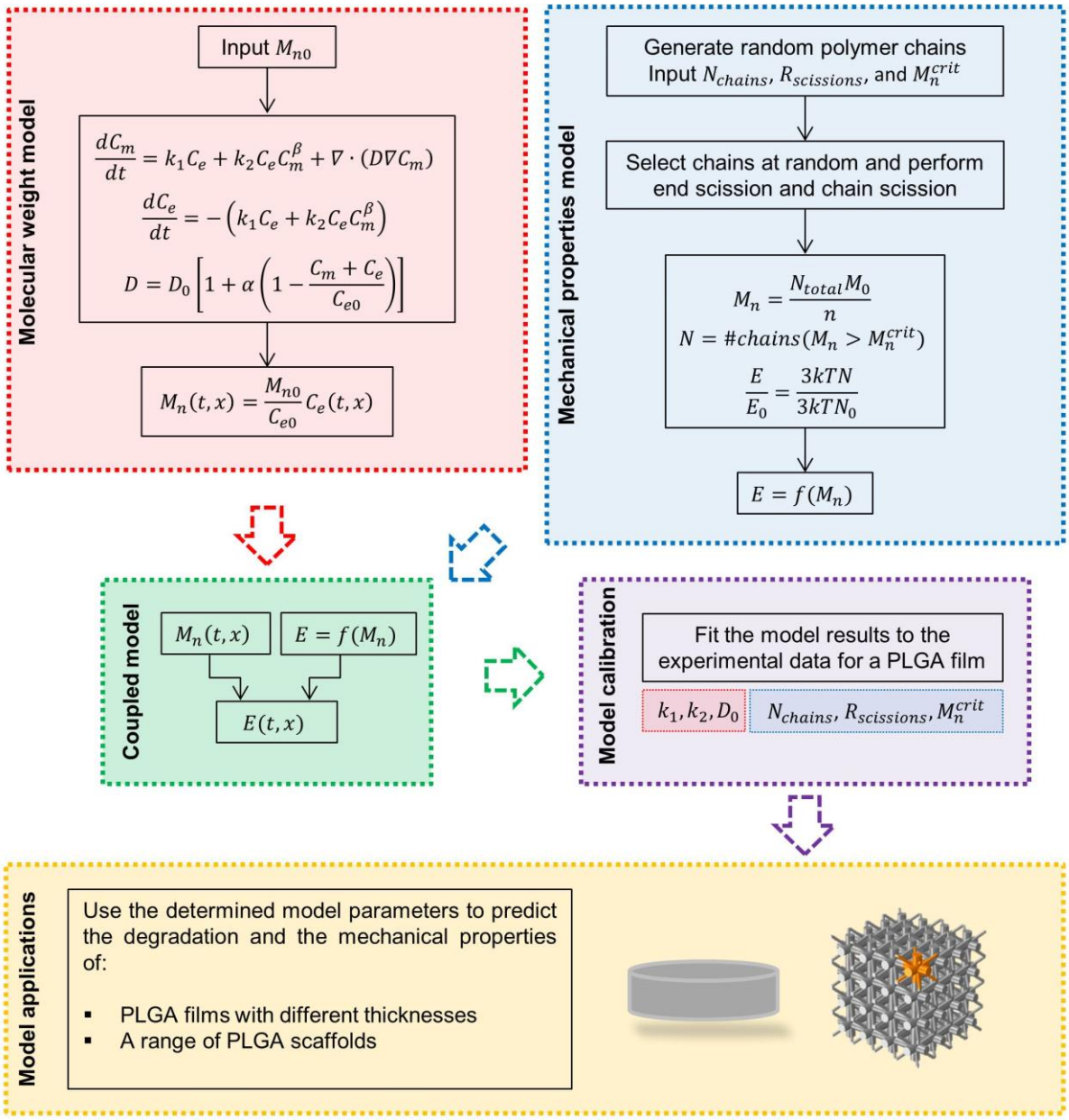

Figure 1: Flowchart of numerical simulation used for degradation behaviour and mechanical properties of PLGA films and tissue engineering scaffolds.

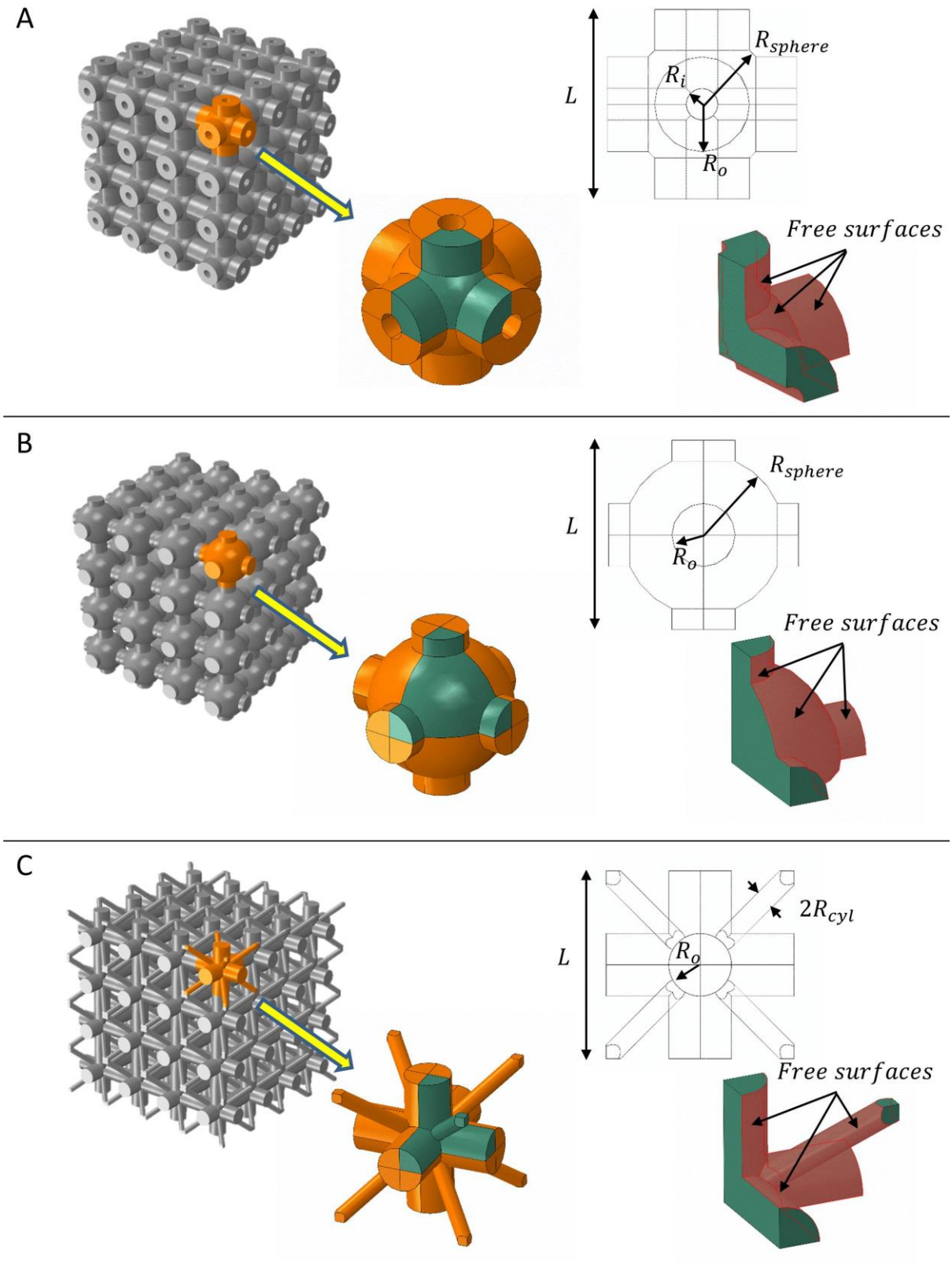

Figure 2: Representative volume element (in green), unit cell (in orange), and geometry of A) Scaffold A, B) Scaffold B, and C) Scaffold C. The red colour shows the free surfaces in contact with the aqueous medium.

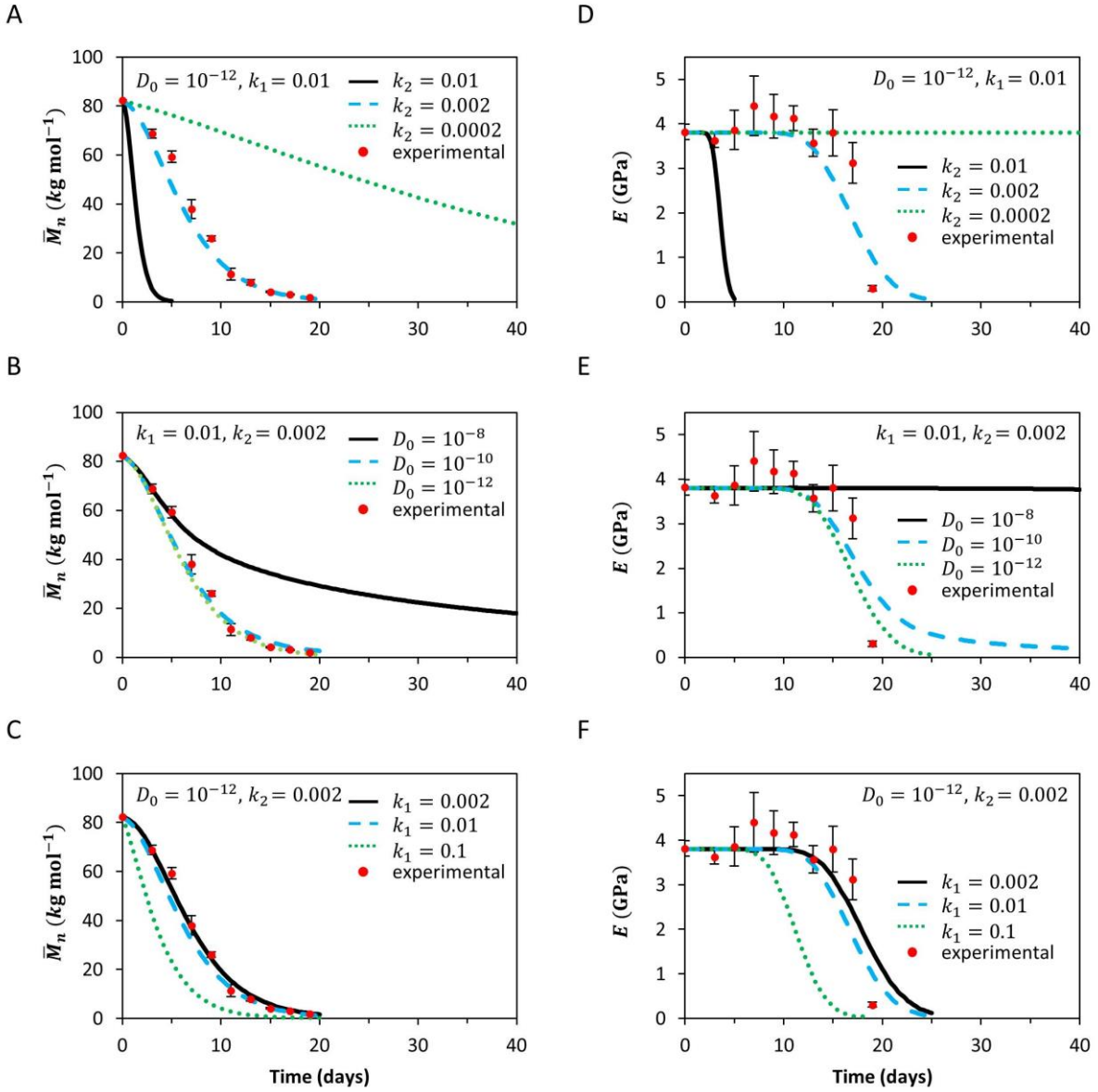

Figure 3: Model fittings of volume-averaged molecular weight ($\bar{M}_n$) (A, B, C) and Young's modulus (E) (D, E, F) to the PLGA film experimental data obtained by Shirazi *et al*. (2014) for different values of k_2 (A, D), D_0 (B, E), and k_1 (C, F). The best fitting to both experimental data for $\bar{M}_n$ and E was achieved by β=0.5, k_1=0.002 day^{-1}, k_2=0.002 (m^3 mol^{-1})$^{0.5}$ day^{-1}, and D_0=10^{-12} m^2 day^{-1}.

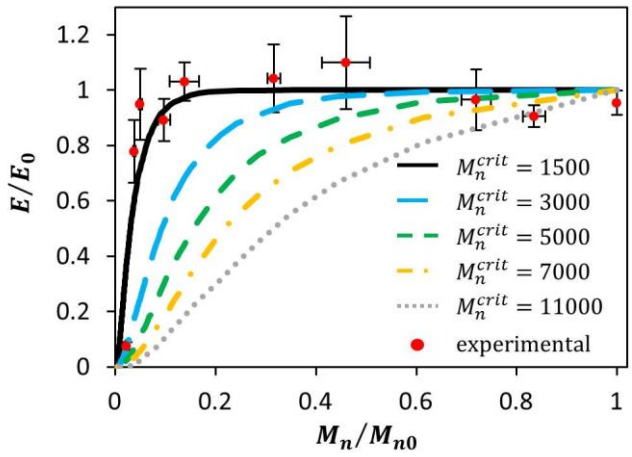

Figure 4: Normalised Young's modulus (E/E_0) versus normalised number average molecular weight (M_n/M_{n0}) for different values of the critical molecular weight (M_n^{crit}) in comparison with the experimental data (red discrete dots) obtained by Shirazi *et al.* (2014) for a PLGA film.

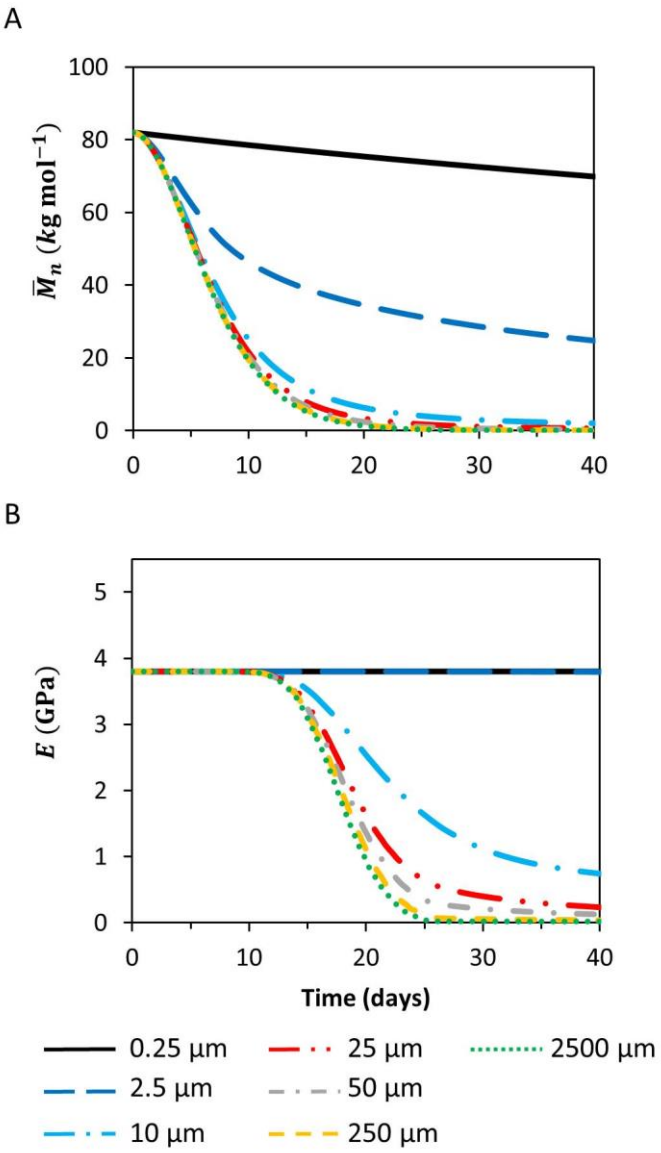

Figure 5: A) Volume-averaged molecular weight ($\bar{M}_n$) and B) Young's modulus (E) for PLGA films of different thicknesses during degradation. The effect of thickness on the Young's modulus for PLGA films with thicknesses of smaller than 2.5 µm is significant.

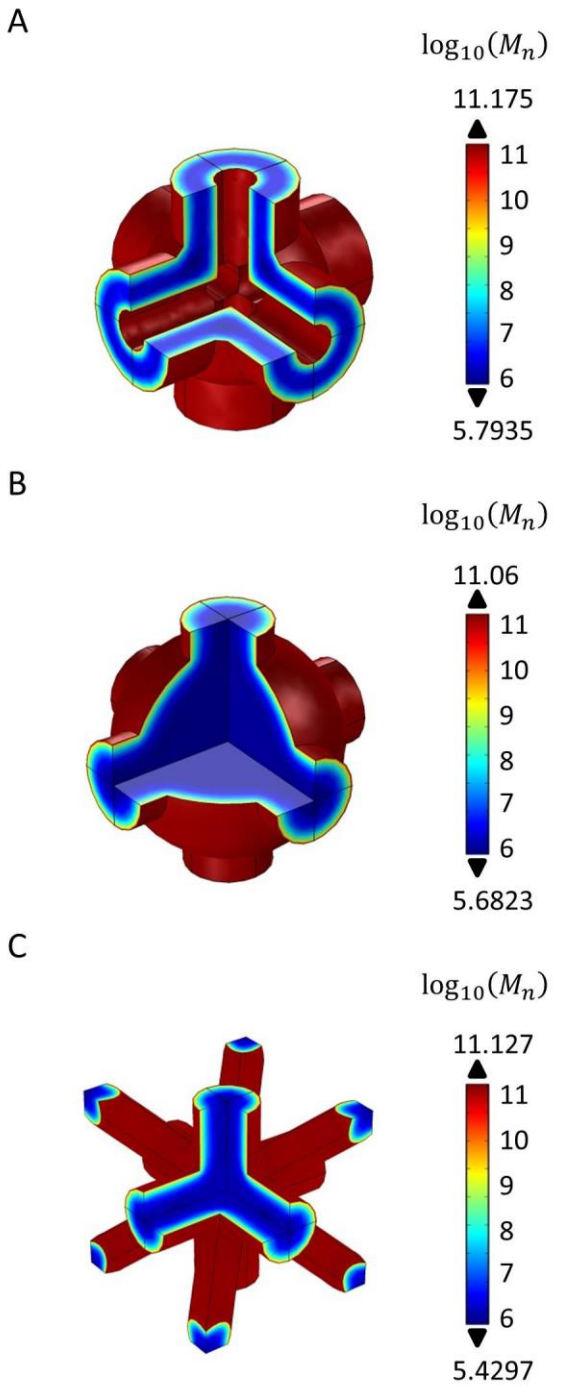

Figure 6: Distribution of molecular weight (M_n) for A) Scaffold A, B) Scaffold B, and C) Scaffold C with 0.05 mm strut thickness after 25 days of degradation shown on a log scale.

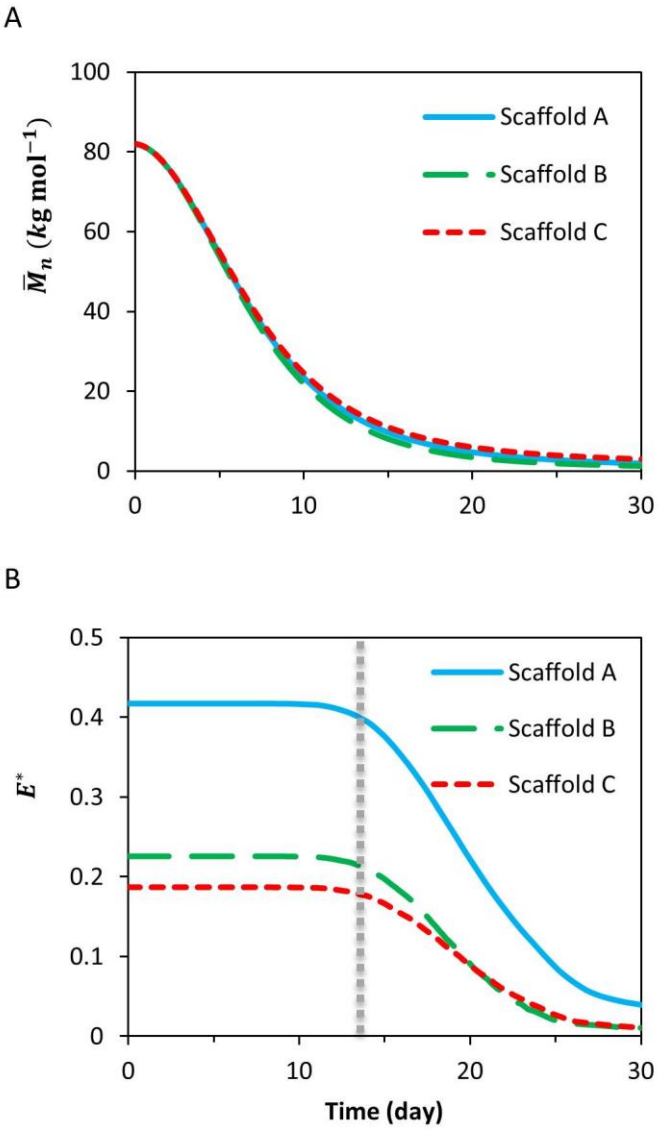

Figure 7: Comparison of A) Volume-averaged molecular weight ($\bar{M}_n$) and B) normalised effective modulus ($E^* = E_{effective}/E_0$) for a different PLGA scaffolds with a strut sizes of 0.05 mm. The grey dashed line indicates that the scaffolds collapse at approximately the same time (~13 days).

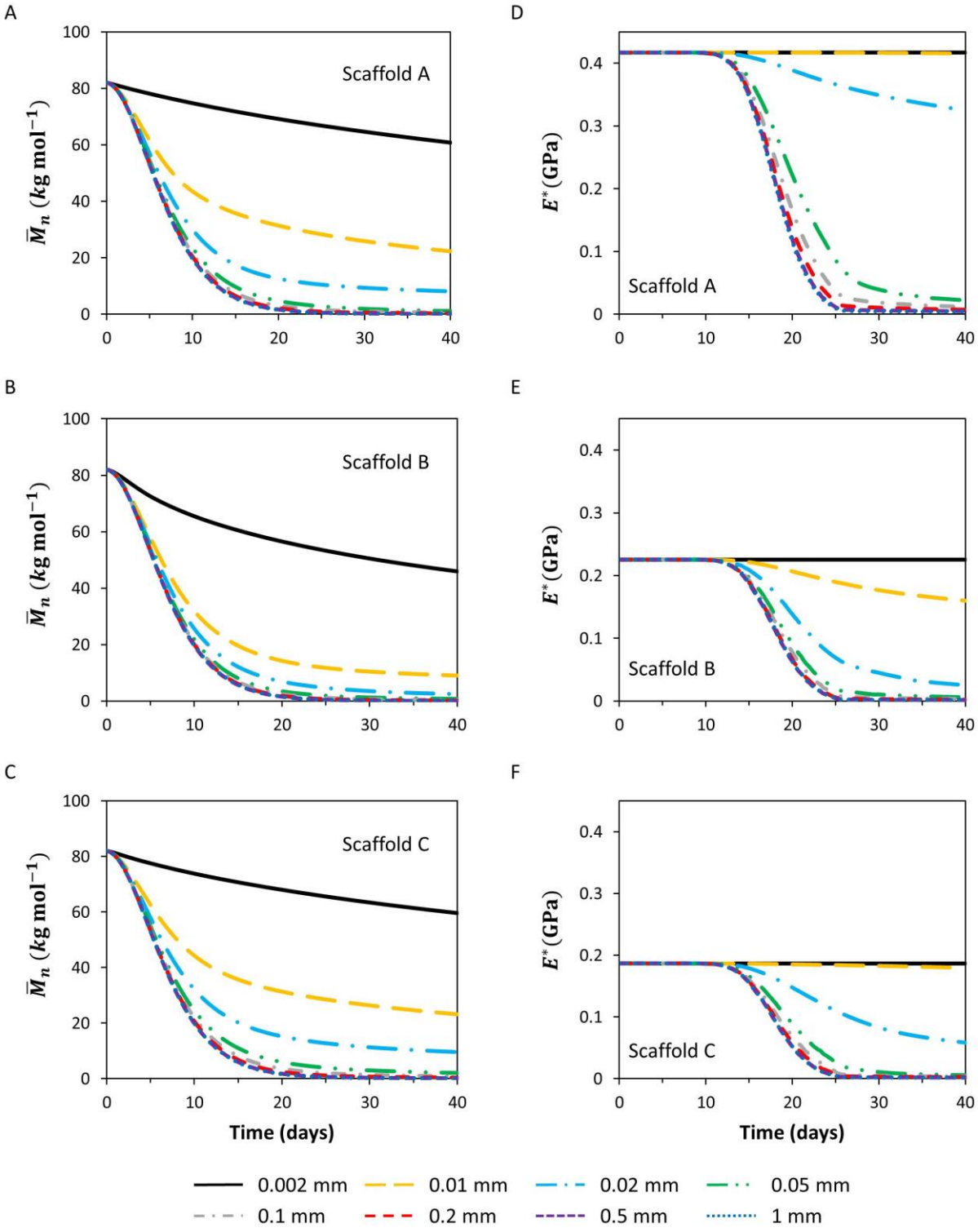

Figure 8: Volume-averaged molecular weight ($\bar{M}_n$) (A, B, C) and normalised effective modulus ($E^* = E_{effective}/E_0$) (D, E, F) for PLGA scaffolds with different architectures and strut sizes. The decrease in effective modulus was significantly different for the struts thinner than 0.02mm.

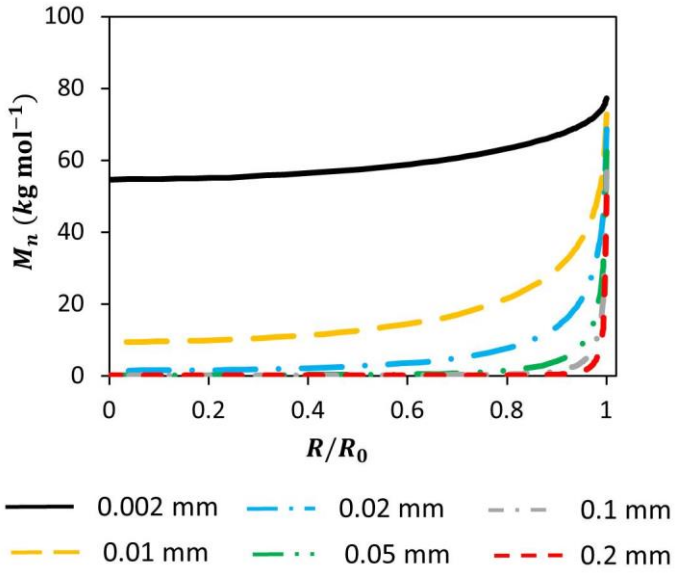

Figure 9: Variation of molecular weight (M_n) for scaffold B with different struts sizes through the thickness of the strut. R_0 is the radius of the strut.

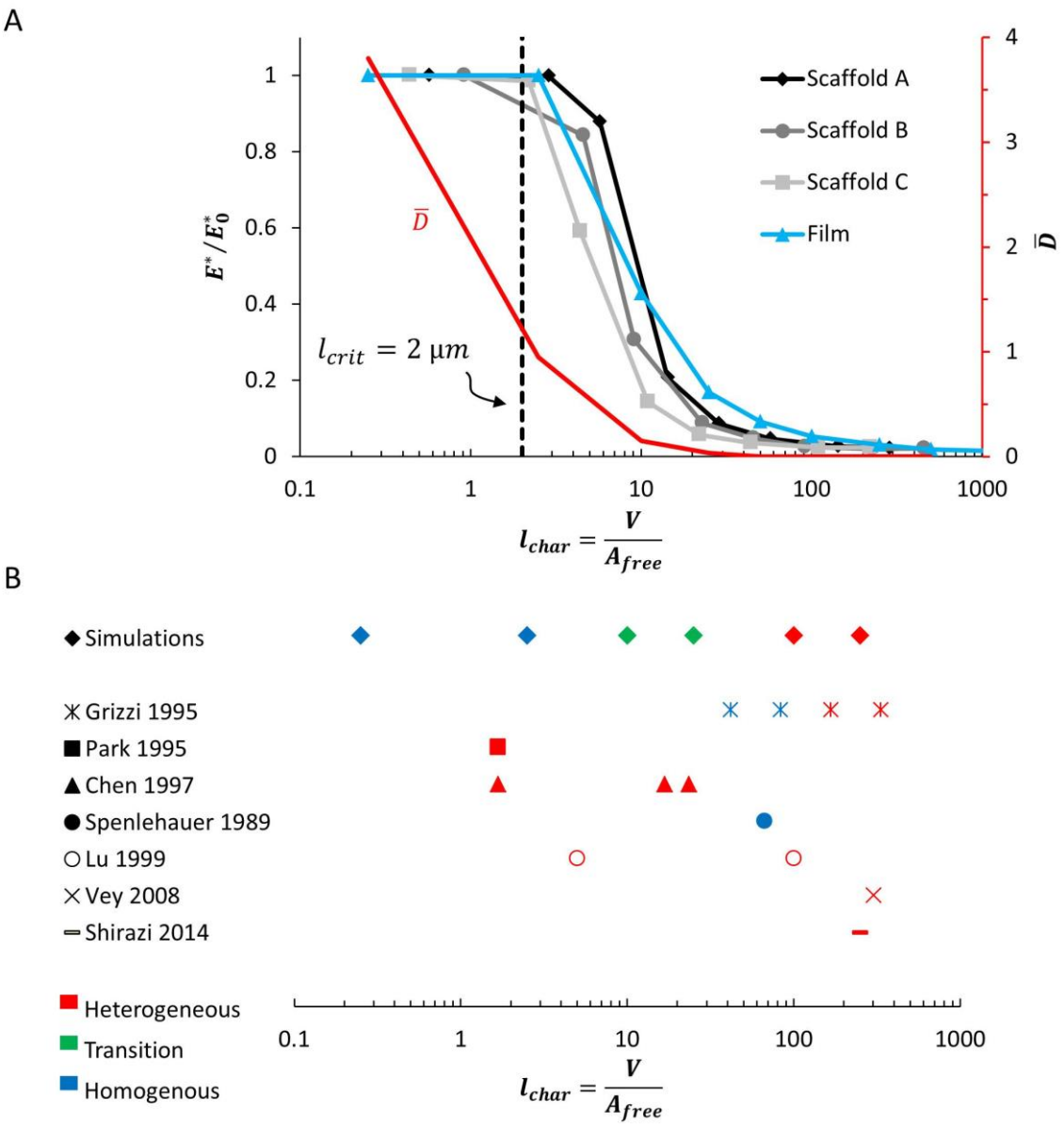

Figure 10: A) the relative change in effective modulus (E^*/E_0^*) after 25 days for different sizes of each scaffold and the dimensionless diffusion coefficient ($\bar{D}$) versus the characteristic length ($l_{char} = V/A_{free}$) for different scaffold architectures and films with different thicknesses. B) Comparison of homogenous, heterogeneous, and transition regimes between the simulations performed in the current study and the experimental observations in the literature.

References

Bucklen, B.S., Wettergreen, W.A., Yuksel, E., Liebschner, M.A.K., 2008. Bone-derived CAD library for assembly of scaffolds in computer-aided tissue engineering. Virtual and Physical Prototyping 3, 13-23.

Chen, L., Apte, R.N., Cohen, S., 1997. Characterization of PLGA microspheres for the controlled delivery of IL-1α for tumor immunotherapy. Journal of Controlled Release 43, 261-272.

Chen, Y., Zhou, S., Li, Q., 2011. Mathematical modeling of degradation for bulk-erosive polymers: Applications in tissue engineering scaffolds and drug delivery systems. Acta Biomaterialia 7, 1140-1149.

Cheng, L., Sun, X., Hu, C., Jin, R., Sun, B., Shi, Y., Zhang, L., Cui, W., Zhang, Y., 2013. In vivo inhibition of hypertrophic scars by implantable ginsenoside-Rg3-loaded electrospun fibrous membranes. Acta Biomaterialia 9, 9461-9473.

Cui, W., Li, X., Zhou, S., Weng, J., 2008. Degradation patterns and surface wettability of electrospun fibrous mats. Polymer Degradation and Stability 93, 731-738.

Dunne, M., Corrigan, O.I., Ramtoola, Z., 2000. Influence of particle size and dissolution conditions on the degradation properties of polylactide-co-glycolide particles. Biomaterials 21, 1659-1668.

Ford Versypt, A.N., Pack, D.W., Braatz, R.D., 2013. Mathematical modeling of drug delivery from autocatalytically degradable PLGA microspheres — A review. Journal of Controlled Release 165, 29-37.

Grayson, A.C.R., Cima, M.J., Langer, R., 2005. Size and temperature effects on poly(lactic-co-glycolic acid) degradation and microreservoir device performance. Biomaterials 26, 2137-2145.

Grizzi, I., Garreau, H., Li, S., Vert, M., 1995. Hydrolytic degradation of devices based on poly(dl-lactic acid) size-dependence. Biomaterials 16, 305-311.

Harada, N., Watanabe, Y., Sato, K., Abe, S., Yamanaka, K., Sakai, Y., Kaneko, T., Matsushita, T., 2014. Bone regeneration in a massive rat femur defect through endochondral ossification achieved with chondrogenically differentiated MSCs in a degradable scaffold. Biomaterials 35, 7800-7810.

Hayman, D., Bergerson, C., Miller, S., Moreno, M., Moore, J.E., 2014. The Effect of Static and Dynamic Loading on Degradation of PLLA Stent Fibers. Journal of Biomechanical Engineering 136, 081006-081006.

Heljak, M.K., Święszkowski, W., Lam, C.X.F., Hutmacher, D.W., Kurzydłowski, K.J., 2012. Evolutionary design of bone scaffolds with reference to material selection. International Journal for Numerical Methods in Biomedical Engineering 28, 789-800.

Lu, L., Garcia, C.A., Mikos, A.G., 1999. In vitro degradation of thin poly(DL-lactic-co-glycolic acid) films. Journal of Biomedical Materials Research 46, 236-244.

Luxner, M., Stampfl, J., Pettermann, H., 2005. Finite element modeling concepts and linear analyses of 3D regular open cell structures. Journal of Materials Science 40, 5859-5866.

Pamula, E., Menaszek, E., 2008. In vitro and in vivo degradation of poly(L-lactide-co-glycolide) films and scaffolds. Journal of Materials Science: Materials in Medicine 19, 2063-2070.

Park, T.G., 1995. Degradation of poly(lactic-co-glycolic acid) microspheres: effect of copolymer composition. Biomaterials 16, 1123-1130.

Ren, T., Ren, J., Jia, X., Pan, K., 2005. The bone formation in vitro and mandibular defect repair using PLGA porous scaffolds. Journal of Biomedical Materials Research Part A 74A, 562-569.

Sackett, C.K., Narasimhan, B., 2011. Mathematical modeling of polymer erosion: Consequences for drug delivery. International Journal of Pharmaceutics 418, 104-114.

Saito, E., Liao, E.E., Hu, W.-W., Krebsbach, P.H., Hollister, S.J., 2013. Effects of designed PLLA and 50:50 PLGA scaffold architectures on bone formation in vivo. Journal of Tissue Engineering and Regenerative Medicine 7, 99-111.

Saito, E., Liu, Y., Migneco, F., Hollister, S.J., 2012. Strut size and surface area effects on long-term in vivo degradation in computer designed poly(l-lactic acid) three-dimensional porous scaffolds. Acta Biomaterialia 8, 2568-2577.

Shirazi, R.N., Aldabbagh, F., Erxleben, A., Rochev, Y., McHugh, P., 2014. Nanomechanical properties of poly(lactic-co-glycolic) acid film during degradation. Acta Biomaterialia.
Soares, J.S., Rajagopal, K.R., Moore Jr, J.E., 2010. Deformation-induced hydrolysis of a degradable polymeric cylindrical annulus. Biomechanics and Modeling in Mechanobiology 9, 177-186.
Spenlehauer, G., Vert, M., Benoit, J.P., Boddaert, A., 1989. In vitro and In vivo degradation of poly(D,L lactide/glycolide) type microspheres made by solvent evaporation method. Biomaterials 10, 557-563.
Uematsu, K., Hattori, K., Ishimoto, Y., Yamauchi, J., Habata, T., Takakura, Y., Ohgushi, H., Fukuchi, T., Sato, M., 2005. Cartilage regeneration using mesenchymal stem cells and a three-dimensional poly-lactic-glycolic acid (PLGA) scaffold. Biomaterials 26, 4273-4279.
Vey, E., Rodger, C., Meehan, L., Booth, J., Claybourn, M., Miller, A.F., Saiani, A., 2012. The impact of chemical composition on the degradation kinetics of poly(lactic-co-glycolic) acid copolymers cast films in phosphate buffer solution. Polymer Degradation and Stability 97, 358-365.
Vey, E., Roger, C., Meehan, L., Booth, J., Claybourn, M., Miller, A.F., Saiani, A., 2008. Degradation mechanism of poly(lactic-co-glycolic) acid block copolymer cast films in phosphate buffer solution. Polymer Degradation and Stability 93, 1869-1876.
Vieira, A.C., Guedes, R.M., Tita, V., 2014. Constitutive modeling of biodegradable polymers: Hydrolytic degradation and time-dependent behavior. International Journal of Solids and Structures 51, 1164-1174.
Vieira, A.C., Vieira, J.C., Ferra, J.M., Magalhães, F.D., Guedes, R.M., Marques, A.T., 2011. Mechanical study of PLA–PCL fibers during in vitro degradation. Journal of the Mechanical Behavior of Biomedical Materials 4, 451-460.
Wang, Y., Han, X., Pan, J., Sinka, C., 2010. An entropy spring model for the Young's modulus change of biodegradable polymers during biodegradation. Journal of the Mechanical Behavior of Biomedical Materials 3, 14-21.
Wang, Y., Pan, J., Han, X., Sinka, C., Ding, L., 2008. A phenomenological model for the degradation of biodegradable polymers. Biomaterials 29, 3393-3401.
Ward, I.M., Sweeney, J., 2012. Mechanical Properties of Solid Polymers. Wiley.
Wettergreen, M.A., Bucklen, B.S., Starly, B., Yuksel, E., Sun, W., Liebschner, M.A.K., 2005. Creation of a unit block library of architectures for use in assembled scaffold engineering. Computer-Aided Design 37, 1141-1149.
Witt, C., Kissel, T., 2001. Morphological characterization of microspheres, films and implants prepared from poly(lactide-co-glycolide) and ABA triblock copolymers: is the erosion controlled by degradation, swelling or diffusion? European Journal of Pharmaceutics and Biopharmaceutics 51, 171-181.
Wu, L., Ding, J., 2005. Effects of porosity and pore size on in vitro degradation of three-dimensional porous poly(D,L-lactide-co-glycolide) scaffolds for tissue engineering. Journal of Biomedical Materials Research Part A 75A, 767-777.